Advances in Medical Sciences 63 (2018) 257–264

Contents lists available at ScienceDirect

Advances in Medical Sciences

journal homepage: www.elsevier.com/locate/advms

Original research article

Aspartic acid functionalized PEGylated MSN@GO hybrid as an effective and sustainable nano-system for *in-vitro* drug delivery

Reza Rahmatolahzadeh[a,*], Masood Hamadanian[a,b], Leila Ma'mani[c], Abbas Shafiee[d]

[a] Institute of Nanoscience and Nanotechnology, University of Kashan, Kashan, Iran
[b] Department of Physical Chemistry, Faculty of Chemistry, University of Kashan, Kashan, Iran
[c] Department of Nanotechnology, Agricultural Biotechnology Research Institute of Iran (ABRII), Agricultural Research, Education and Extension Organization (AREEO), Karaj, Iran
[d] Department of Medicinal Chemistry, Faculty of Pharmacy and Pharmaceutical Sciences Research Center, Tehran University of Medical Sciences, Tehran, Iran

ARTICLE INFO

Keywords:
Breast cancer cell
Curcumin delivery
Graphene oxide
Mesoporous silica nanoparticles pH sensitive

ABSTRACT

Purpose: In this research, aspartic acid functionalized PEGylated mesoporous silica nanoparticlesgraphene oxide nanohybrid (As-PEGylated-MSN@GO) prepared as a pH-responsive drug carrier for the curcumin delivery. For better camouflage during blood circulation, poly(ethylene glycol) was decorated on the surface of MSN@GO nanohybrid.

Materials and methods: The nanocarrier was characterized by using X-ray powder diffraction (XRD), dynamic light scattering (DLS), UV–vis spectroscopy, thermal gravimetry analysis (TGA), FT-IR, SEM and TEM.

Results: The size of modified MSN@GO was around 75.8 nm and 24% wt. of curcumin was loaded on the final nanohybrid. pHdecrement from 7.4 to 5.8 the release medium led to increase the cumulative amount of drug release from 54% to 98%.

Conclusions: As-functionalized MSN@GO had no cytotoxicity against human breast adenocarcinoma (MCF-7) and human mammary epithelial (MCF10A) as cancerous and normal cell lines, respectively. Whereas curcuminloaded nanohybrid showed excellent killing capability against MCF-7 cells.

1. Introduction

Due to the importance of breast canceras the most common cancer in women, a large number of studies have been devoted to develop applicable and impressive nanocarriers for anticancer delivery to the cancer cells [1]. (Diferuloylmethane)-(1,7-bis(4-hydroxy-3-methoxyphenyl)-1,6-hepadiene-3,5-dione) which is extracted from turmeric Curcuma longa L. rhizomes (Zingiberaceae family), known as curcumin (CUR), is a natural diphenolic compound [2,3]. CUR has valuable pharmaceutical properties including anti-cancer, anti-inflammatory, anti-microbial, anti-oxidant, and anti-fungal activities [4–9]. Unfortunately, CUR is considered as a hydrophobic drug and poor bioavailability, low solubility, absorption with rapid elimination are some limitations for the pharmaceutical applications of this drugIn addition, the use of therapeutical activities of this drug has been extremely challenging. Therefore, a large number of researchers have focused on developing an efficient nano-drug delivery system (DDS) for appropriate CUR transport and delivery [10,11].

Among various carbon materials, graphene has an unique structure that can be employed in various applications (*e.g.* biosensors, nanoelectronic, and transparent electrodes). Graphene is a flexible layered structure that has large specific surface area with aromatic sp^2 domains [12–14]. The oxidized form of graphene, graphene oxide (GO), contains carboxyl, epoxy and hydroxyl functional groups in its basal sheets and edges in which can be functionalized with biomolecules and drugs for *in vitro* and *in vivo* biological applications [15–18].

Among various materials that are employed as a support, mesoporous silica nanoparticles (MSNs) have gained great interest and are considered as "reliable support or carrier materials". MSNs present appropriate ability and efficiency for various biomedical applications [19]. Ordered structure, high pore volume, high surface area, suitable hydrothermal stability and appropriate biocompatibility are some unique features of MSNs in which these properties can provide valuable opportunities for designing beneficial DDSs [16,20]. By dispersing mesoporous materials onto the surface of graphene nanolayers, graphene–mesoporous silica composites can be prepared. In these hybrids, the inherent characteristics of graphene and porous material are maintained and also a novel synergistic effect is produced [21–24]. In

* Corresponding author at: Institute of Nanoscience and Nanotechnology, University of Kashan, Ravandi Street, Kashan, Islamic Republic of Iran. Tel.: + (098) 9125630755; Fax: + (098)2164321122.
E-mail address: rezarahmati@khayam.ut.ac.ir (R. Rahmatolahzadeh).

https://doi.org/10.1016/j.advms.2018.01.003
Received 10 May 2017; Accepted 8 January 2018
Available online 20 March 2018

addition, the ability of tailoring the end groups in MSNs offers a considerable range of fine-tuning in drug loading and targeted release properties [25–28].

Surface modification of different nanoparticles and also, nanohybrids can be performed by poly(ethylene glycol) (PEG) chains. PEG presents abundant useful properties such as aqueous solubility, biocompatibility, non-toxicity, non-antigenic and non-immunogenic characteristics [29]. Covalent attachment of PEG on the surface of nanoparticles (covalently PEGylation) can result in reducing the blood interaction (low plasma protein binding) and also, can be assumed as an appropriate manner to improve permeability, retention effect, EPR effect and colloidal stability in aqueous media [30].

In this research, mesoporous silica nanoparticles have been combined with graphene oxide and then, modifed by PEG. After that, CUR was used to functionalize PEGylated mesoporous silica nanoparticles-graphene oxide hybrid as an appropriate candidate for the *in vitro* cancer treatment.

2. Material and methods

2.1. Chemicals, cell lines and cell culture

Tetraethylorthosilicate (TEOS, 98%), 3-(4,5-Dimethylthiazol-z-yl)-2,5-diphenyltetrazotium bromide (MTT), 3-(triethoxysilyl)propyl isocyanate (TESPIC), dimethyl sulfoxide (DMSO) and curcumin were purchased from Sigma. EDTA, phosphate buffer (20 mM, pH 7.8) and corresponding salts used throughout this research were purchased from Merck. Trypsin, culture medium (DMEM = Dulbecco's Modified Eagle's Medium) and supplements were obtained from Gibco (Germany). MCF-7 (human breast adenocarcinoma) was purchased from Pasteur Institute (Tehran, Iran). The cell lines were grown in DMEM medium supplemented with 10% (v/v) heat-inactivated fetal bovine serum (FBS), 2% l-glutamine, 2.7% sodium bicarbonate, 1% Hepes buffer and 1% penicillin-streptomycin solution (GPS, Sigma) at 37 °C in humidified atmosphere with 5% CO_2. All cells were trypsinized in the solution of 0.05% trypsin and seeded into 96-well micro-plates at the density of 1×10^5 cells/well.

2.2. Characterization

XRD spectrum was recorded at room temperature with a Philips X'pert 1710 diffractometer using CuKα (α = 1.54056 Å) in the Bragg-Brentano geometry. Morphological studies were also performed by using FE-SEM (Hitachi S-4800 II, Japan). Ultraviolet–visible spectra of the nanoparticles were recorded by using UV–vis Jasco-530. The TEM analyses were performed on a Hitachi H-7650 (Tokyo, Japan) operating at an acceleration voltage of 80 kV. FT-IR spectra were taken by using Nicolet FT-IR Magna 550 spectrographs with spectroscopic grade KBr. BET and BJH methods were employed to calculate surface area and pore size distribution,respectively. Size of nanoparticles was assessed by dynamic light scattering (Nano-ZS 90, Malvern Instrument, United Kingdom). In addition, zeta potential of nanoparticles was also calculated in folded capillary cells (ZetasizerNano ZS90, Malvern Instruments Ltd., Malvern, UK).

2.3. Preparation of nanocarrier

2.3.1. Preparation mesoporous silica nanoparticle-graphene oxide hybrid (MSN@GO)

At first, GO was synthesized according to our prior report by modified Hummers method [31]. Graphite (1 g) was added to a solution of H_2SO_4 (50 mL, 96%) in an ice bath and then, $KMnO_4$ (2 g) was added to the solution. The reaction mixture was left to flick for 3 h (the temperature of solution kept under 10 °C and continued by another 30 min at 35 °C). After that, the product was diluted with 50 mL of deionized water (temperature was kept under 100 °C) and was shaked for 30 min. The product was further diluted by deionized water (total volume of solution is around 100 mL). In the next step, H_2O_2 (30%, 10 mL) was added to the mixture. The final solid was separated and washed thoroughly with HCL solution (5%). Exfoliation of graphite oxide dispersion by ultrasonic waves, filtration and drying of product at 70 °C resulted in GO powder.

MSN@GO hybrid was synthesized by using GO and TEOS according to the previous report with slight modification [32]. At first, CTAB (8 g) and NaOH (0.2 g) were added to 400 mL of deionized water. The solution was combined with a suspension containing GO (450 mg, pH = 8.5). Then, TEOS (6 mL) dissolved in EtOH (10 mL) and this solution was added drop-wise to the later mixture (under stirring at 70 °C for 12 h). The product was centrifuged and washed thoroughly applying soxhlet with EtOH/HCl (1%). Finally, the final solid was dried in a vacuum oven at 30 °C overnight.

2.3.2. Synthesis of PEGylated MSN-GO nanohybrid (PEGylated MSN@GO NPs)

To prepare PEGylated MSN@GO nanohybrid, PEG-silane as a linker was synthesized according to our previous report [33]. At first, a solution of MSN@GO (0.5 g) in 25 mL EtOH/H_2O (1:3) and HCl (pH = 3.5) was prepared. Then, a solution of PEG-silane (2 g) in EtOH (25 mL) was added drop-wise to previous solution and the final solution was left under stirring for 12 h. Then, the solution was filtered off and washed thoroughly with H_2O/EtOH. Finally, the product was dried at 60 °C in vacuum to obtain PEGylated MSN@GO.

2.3.3. Synthesis of aspartic acid functionalized PEGylated MSN-GO nanohybrid (As-PEGylated MSN@GO NPs)

At first, PEGylated MSN@GO (10 g) was dispersed in dichloromethane (DCM) (100 mL). In addition, a solution of *p*-tosyl chloride (*p*-TsCl, 1 g) in 20 mL of DCM and triethylamine (2 mL) was added drop-wise to the later solution and the reaction was stirred at 30 °C for 12 h. The solid residue was separated by a centrifuge and washed thoroughly with hot de-ionized water and acetone to remove salt and organic impurities. Finally, it was dried for 12 h at 70 °C in vacuum to give tosyl-PEGylated MSN@GO. Then, 0.5 g of tosyl-PEGylated MSN@GO was ultrasonically dispersed in acetonitrile (25 mL) for 30 min 30 °C and a solution of aspartic acid (0.3 g in 20 mL of DCM) was added to the later mixture and stirred vigorously at 80 °C overnight. The residual solid was centrifuged, washed with hot EtOH and dried under vacuum to obtain aspartic acid functionalized PEGylated mesoporous silica nanoparticle-graphene oxide nanohybrid.

2.4. Drug loading

In order to investigate the loading capability, a solution of CUR was added to 100 mg of As-PEGylated MSN@GO in acetone and put under argon atmosphere overnight. Then, the solid was obtained by a centrifuge at 11,000 rpm. After that, unlinked CUR was removed by washing with EtOH and the product was dried to give CUR@[As-PEGylated MSN@GO] nanohybrid. The residual CUR content could be measured by UV–vis spectrophotometry of extracted solution from both supernatant and washed solutions and therefore, loading efficiency of CUR could be achieved.

2.5. Drug release profile

The release of CUR from As-PEGylated MSN@GO nanohybrid was measured at given time intervals (0–120 h). To investigate the *in vitro* release, phosphate buffer solutions (pH 7.4 and 5.8) were used as normal and acidic pH (at 37 °C), respectively. Therefore, 10 mg of CUR@[As-PEGylated MSN@GO] nanohybrid was entranced to a dialysis bag with cut-off 3500 g mol^{-1} and soaked into 200 mL of phosphate buffer solution (PBS) (0.01 M, pH = 7.4 and 5.8). Sampling of buffer solution was carried out in 0, 2, 4, 8, 12, 24, 36, 48, 72, 96, and

120 h. After each sampling, 1.0 mL of samples was collected and the medium was charged with 1.0 mL of fresh buffer solution. Determination of CUR was performed by fluorescence spectroscopy (450 nm).

2.6. Particle size and zeta potential

DLS is a non-invasive technique for measuring the size of particles and molecules in various suspensions. DLS and zeta-potential measurements were employed to determine the size distribution, average sizeand charge distribution of freeze-dried CUR@[As-PEGylated MSN@GO] nanohybrid.

2.7. Cell viability assay

To study the cytotoxicity of CUR, As-PEGylated MSN@GO and CUR@[As-PEGylated functionalized MSN@GO] nanohybrid were investigated in MCF-7 and MCF10A as cancerous and normal cell lines,

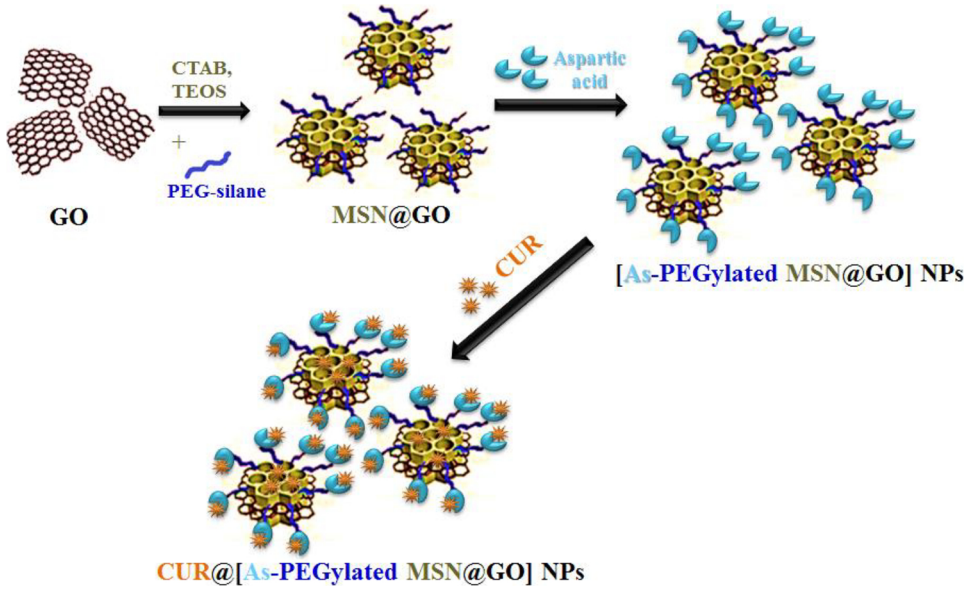

Scheme 1. Synthesis of CUR@[As-PEGylated MSN@GO] NPs.

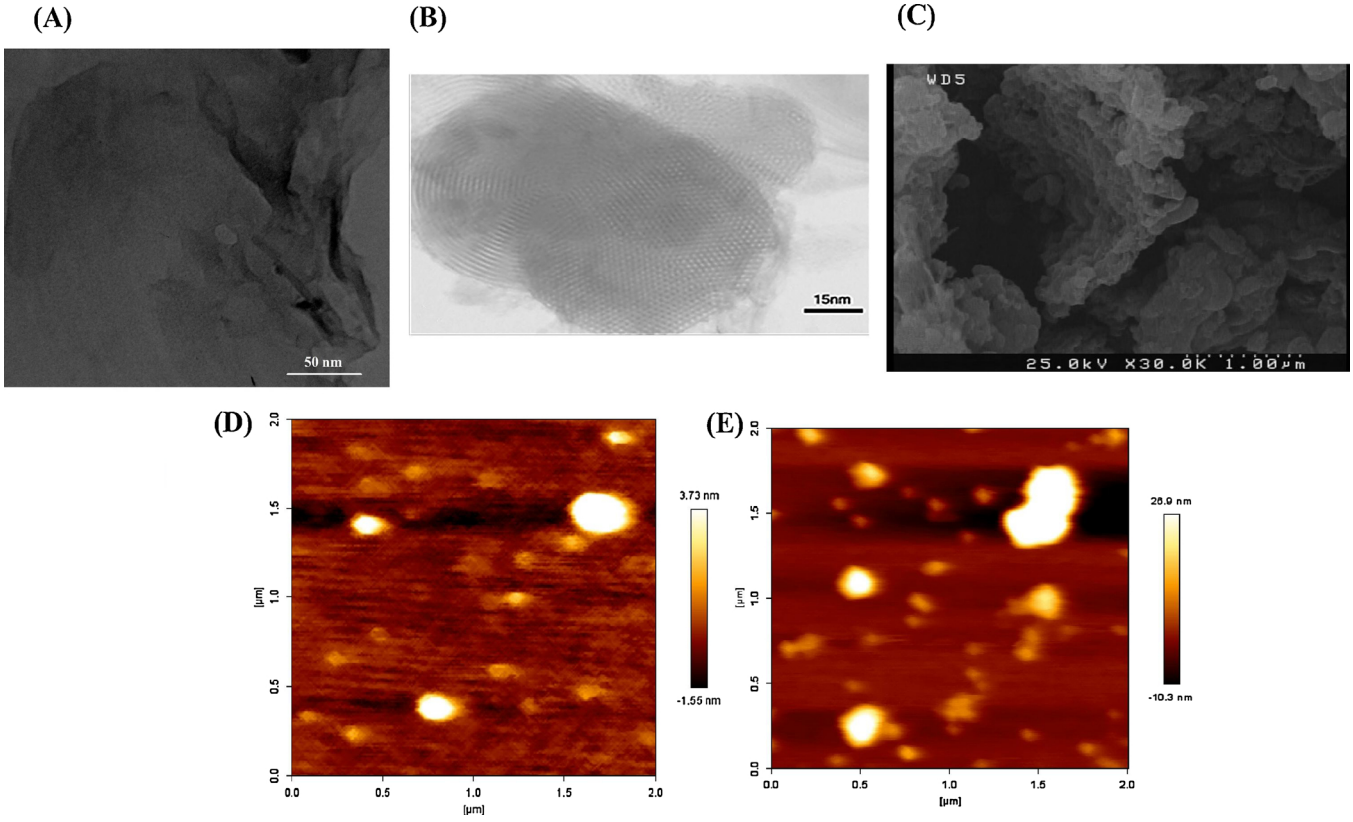

Fig. 1. TEM image of GO (A) and [As-PEGylated MSN@GO] nanohybrid (B); SEM image of [As-PEGylated MSN@GO] nanohybrid (C); and AFM images of [AS-PEGylated @MSN@GO] (D) and CUR[AS-PEGylated @MSN@GO] nanohybrids.

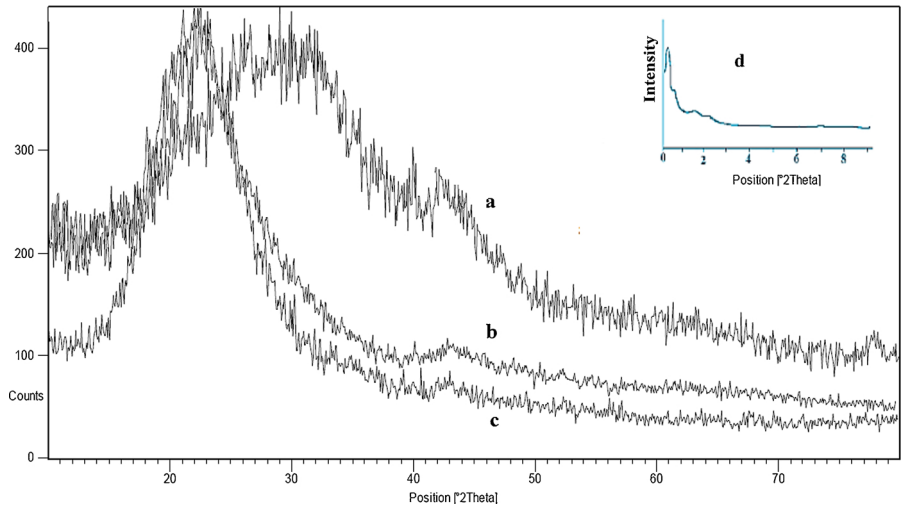

Fig. 2. XRD patterns of a) GO, b) MSN@GO, c and d) high and low angle XRD of MSN@GO.

respectively. To this purpose, the colorimetric analysis was applied to measure the reduction of yellow 3-(4,5-dimethythiazol-2-yl)-2,5-diphenyltetrazolium bromide (MTT) by mitochondrial succinate dehydrogenase. The cell lines were kept in DMEM medium, supplemented with 2 mM of L-cysteine and 10% of FBS and grown at 37 °C in a 5% CO_2 atmosphere. Cells (1×10^4) were seeded in 96-well plates. Then, CUR@[As-PEGylated MSN@GO] nanohybrid was suspended in the complete culture medium to give the final CUR concentrations of 10 to 60 µM, and then added to the cells. After 12, 24, 48 and 72 h of exposure, the culture media was removed and the cells were washed twice with PBS and then, 20 µL of MTT (5 mg/mL) was added to each well. Plates were incubated for 3 h at 37 °C. Afterward, 100 µL of DMSO was added to each well and left at 37 °C for 15 min and the optical density was measured at 595 nm using a microplate reader (Biotek, USA). The results were normalized with control and were expressed as the mean absorbance of ± SEM of three independent biological replicates.

2.8. Cellular uptake investigation

To investigate the cellular uptake of CUR@[As-PEGylated MSN@GO] nanohybrid in MCF-7 human breast adenocarcinoma cells, 2×10^5 cells were seeded in 6-well plates in 3 mL medium (DMEM) under standard culture conditions. After 12 h incubation and cell attachment, media was replaced with 3 mL of serum-free medium containing 50 µg/mL free CUR or CUR loaded nanohybrid loaded and incubated for 6 h. The cells were washed twice with PBS to remove the complexes present in the medium and the cell were analysed with spectrofluorophotometer to measure the cellular uptake of the CUR@[As-PEGylated MSN@GO] nanohybrid. Excitation and emission wavelengths were 420 nm and 470 nm, respectively.

3. Results and discussion

3.1. Illustration of drug delivery system

Scheme 1 presents the general procedure for the preparation of designed nano-carrier [As-PEGylated MSN@GO]. In the first step, the synthesized porous frameworks were characterized by XRD, N_2 adsorption-desorption isotherms, FT-IR, TGA, TEM, and SEM. Fig. 1a presents TEM image of MSN@GO and [As-PEGylated MSN@GO], respectivly. According to these images, porous framework of nanohybrid could be easly observed. Also, the mesoporous structure can be concluded by estimating the pore size in these images. In addition, TEM images illustrate that mesoporous silica was widely covered with thin transparent GO nanolayers. SEM image of MSN@GO and [As-PEGylated

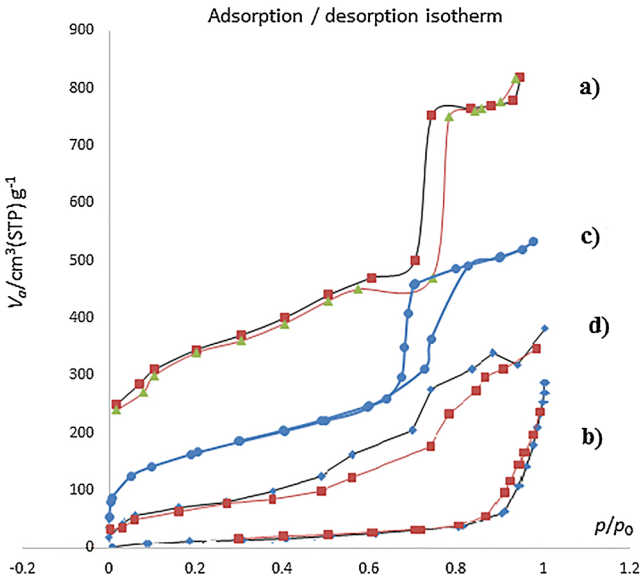

Fig. 3. Nitrogen adsorption–desorption isotherm pattern a) SBA-15, b) GO, c)MSN@GO, d) CUR@[As-PEGylated MSN@GO] nanohybrid.

MSN@GO] nanohybrids are shown in Fig. 1c. Atomic force microscopy (AFM) was used to visualize the morphologies of prepared nanohybrids (Figure d and e). AFM images showed the coatings of nanohybrid a corona around of nanohybrids.

The mesoporous-graphene hybrid framework was also evaluated by XRD analtsis. XRD patterns of GO, GO@MSN, and low angle XRD of MSN@GO are shown in Fig. 2a–c, respectively. According to Fig. 2a, the mesporous structure of GO can be confirmed. According to Fig. 2b, the

Table 1
BET and BJH analyses for MSN@GO based materials.

NPs	S_{BET} (m^2g^{-1})	V_{total} (cm^3g^{-1})	Pore diameter (nm, BJH)
GO	110	0.219	10.2
MSN	820	1.510	7.2
MSN@GO	560	0.589	8.03
As-PEGylated MSN@GO	330	0.390	5.3
CUR@[As-PEGylated MSN@GO]	204	0.219	3.2

peak positions have virtually fixed and therefore, the retention of GO scaffold after the manipulation is demonstrated. As seen in Fig. 2c, the low angle XRD pattern confirmed the mesporous matrix.

N_2 adsorption–desorption isotherms were performed to evaluate the nature of nanoparticle surface (Fig. 3). The specific surface area, diameter distribution and total pore volume for solids were measured by multiple-point BET (Brunauer, Emmett and Teller) and BJH (Barrett–-Joyner–Halenda), respectively. According to the results (Table 1), the surface area, pore volume, and pore size decreased after surface functionalization.

FT-IR spectra of MSN@GO, [As-PEGylated MSN@GO] and CUR@[As-PEGylated MSN@GO] nanohybrids are presented in Fig. 4a–c, respectivly. In Fig. 4a, the broad peak at 1103 cm^{-1} revealed that is corresponeded to C—O bond of PEG segment and Si-O bond. The peak at 2885 cm^{-1} resulted from the methylene group. In addition, the broad peaks at 1710 and 3417 cm^{-1} are related to C═O bond and hydroxyl groups in the PEG chains, respectively. Moreovere, the characteristic peaks at 1390 and 1570 cm^{-1} are attributed to the presence of C—N and N—H bonds in PEG-silane. In Fig. 4b, the broad C—O—C band is revealed at 1090 cm^{-1} that is related to the etheric linkages of PEG segments. The peak at 2880 cm^{-1} is originated from the methylene group near to oxygen atom. The broad peak at 3494 cm^{-1} is due to O—H and N—H stretching band of end hydroxyl and amine groups in aspartic acid. Additionally, the characteristic peak at 1388 cm^{-1} is assigned for the presence of C—N bond in the aspartic acid. Finally, the peaks at 1590 and 1650 cm^{-1} are related to N—H and C═C aromatic, repectively. In Fig. 4c, FT-IR spectra of As-PEGylated MSN@GO nanohybrid, the peaks around 1100–1300 cm^{-1} are attributed to Si-O and C—O moieties and the band at 3024 cm^{-1} related to N—H and carboxylic acid.

TGA curves of various MSN@GO samples are presented in Fig. 5. In these thermograms, termprature range of 25 to 600 °C was applied. According to Fig. 5, the first peak at 100 °C is related to desorption of water. The second peak is also related to loss of the organic group. Based on these results, it is found that the loading of PEG and aspartic acid were 33% and 44% wt. The amount of loaded aspartic acid and PEG moieties into MSN@GO scaffold was also confirmed by elemental analysis. Also, TGA analysis of CUR@[As-PEGylated MSN@GO] nanohybrid revealed the weight loss of about 69% that it can be attributed to the elimination of CUR and PEG linker.

The particle size distributions of CUR@[As-PEGylated MSN@GO] nanohybrid (Fig. 6) in PBS solution were determined by DLS technique. According to the results, the particle size distributions were relatively narrow (mean dimmer = 75.8 nm, PDI = 0.081). The obtained PDI

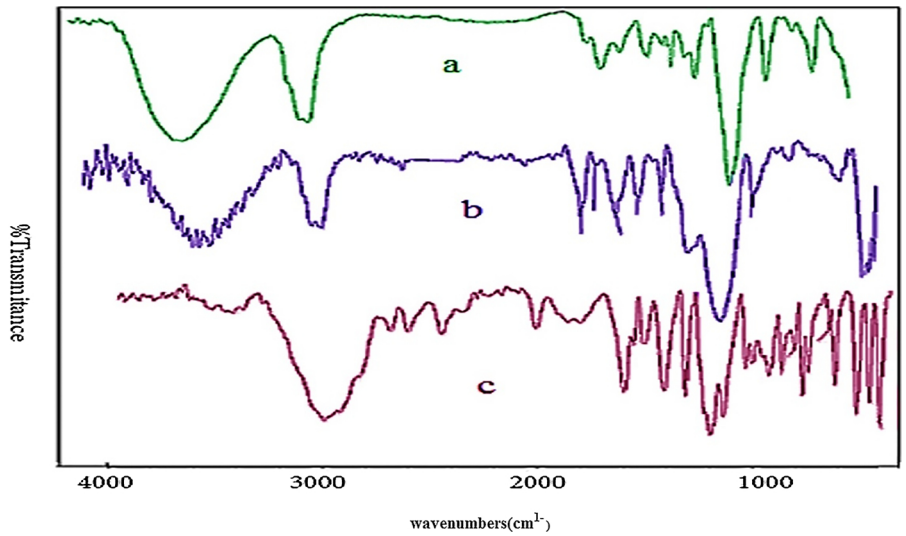

Fig. 4. FT-IR spectra of a) PEGylated MSN@GO, b) PEGylated MSN@GO, and c) As-PEGylated MSN@GO nanohybrid.

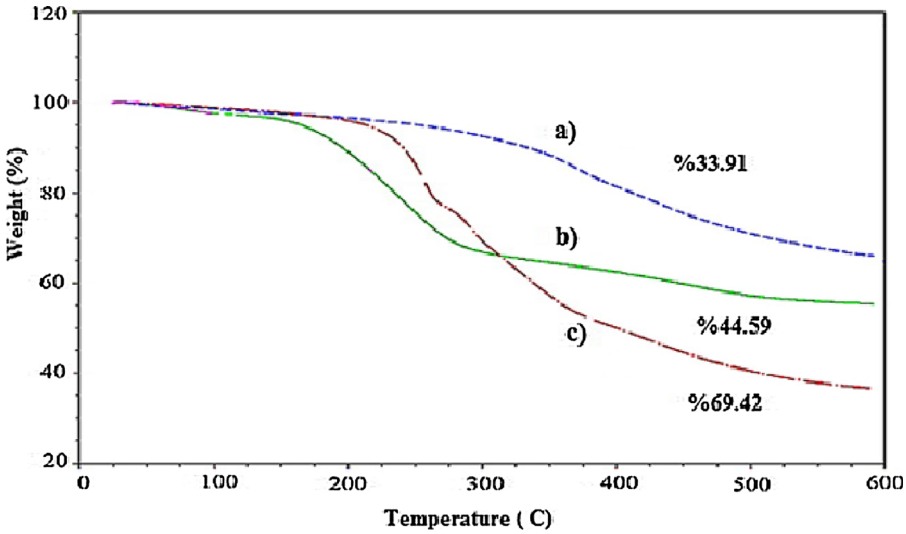

Fig. 5. TGA of a) MSN@GO, b) As-PEGylated MSN@GO, and c) CUR@[As-PEGylated MSN@GO] nanohybrid.

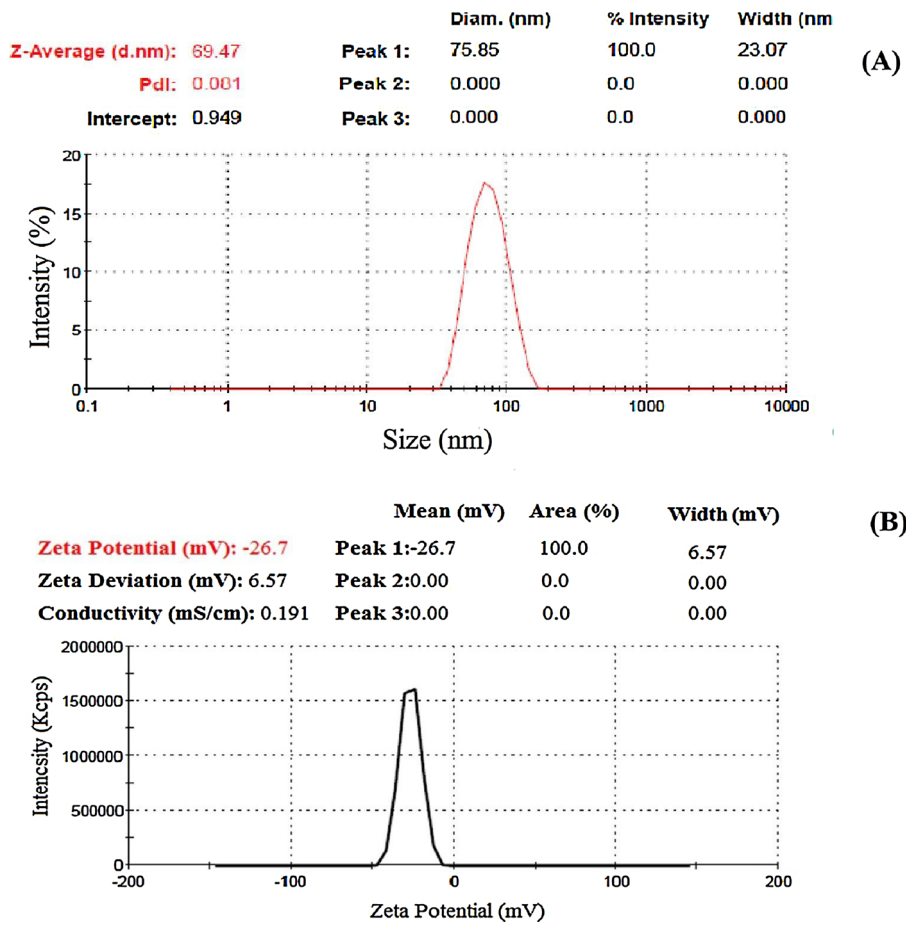

Fig. 6. a) DLS; b) zeta-potential of CUR@[As-PEGylated MSN@GO] nanohybrid.

value showed that MSN@GO has uniform distribution (this is a critical factor in biomedicine applications). The zeta potential for aspartic acid functionalized PEGylated MSN@GO nanohybrid was negative (−26.7 mV). However, zeta potential changed to positive after the loading of CUR on the As-PEGylated functionalized MSN@GO nanohybrid.

3.2. Determination of CUR loading efficiency

To achieve the optimal loading efficiency for the designed nanocarrier, different ratios of [As-PEGylated MSN@GO] nanohybrid and drug were assessed to achieve the desirable efficiency in loading and release. The obtained mixtures were centrifuged at 18000 rpm and supernatant was completely gathered. The amount of CUR remaining in the collected supernatant was then measured by a spectrophotometer at 432 nm, and TGA analysis for obtained CUR loaded nanohybrid. The loading efficiency of CUR was 67 ± 1.5% with proportion of 1.5 mmol: 1 g for CUR@[As-PEGylated MSN@GO] nanohybrid.

Optimal loading efficiency of the designed nanocarrier is an important parameter that can be obtained by evaluating different ratio of As-PEGylated MSN@GO nanohybrid and drug (CUR). The prepared mixture (various ratios of nanocarrier and CUR) were centrifuged at 12000 rpm and supernatant was completely collected. The remained CUR in the collected supernatant was measured by a spectrophotometer at 432 nm. The loading efficiency of CUR@[As-PEGylated functionalized MSN@GO] nanohybrid was 67 ± 1.5% with proportion of 1:1.5 for CUR@[As-PEGylated MSN@GO] nanohybrid.

3.3. In-vitro release of CUR

Fluorescence emission intensity of the supernatant under different pH (7.4 and 5.8) was employed to determine the amount of released drug (CUR) from CUR@[As-PEGylated MSN@GO] nanohybrid. pH values of 7.4 and 5.8 indicate pH of normal blood and cancerous cells environment, respectively. Fig. 7 presents *in vitro* release profiles of CUR@[As-PEGylated MSN@GO] nanohybrid at pH 7.4 and pH 5.8 (at 37 °C). Between pH 7.4 and 5.8, CUR has been released with slower release pattern from CUR@[As-PEGylated MSN@GO] nanohybrid at pH 7.4 (over a 100 h period). In addition, the results indicated CUR release efficiency from CUR@[As-PEGylated MSN@GO] nanohybrid at the first 24 h is about 32.49% and 63.54% (under physiological and acidic

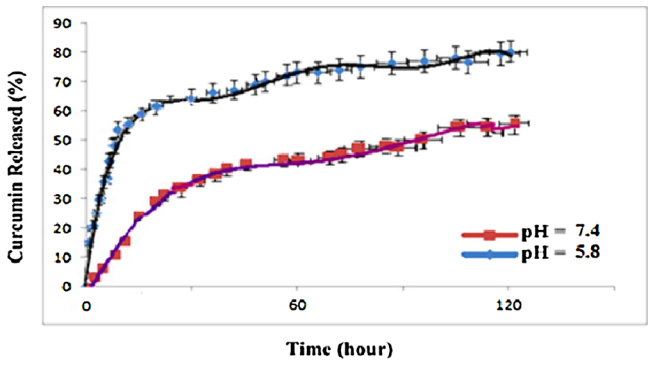

Fig. 7. *In vitro* release profiles of CUR@[As-PEGylated MSN@GO] nanohybrid at pH 7.4 and pH 5.8; all experiments were performed at 37 °C. Data represent mean values ± SD (n = 3).

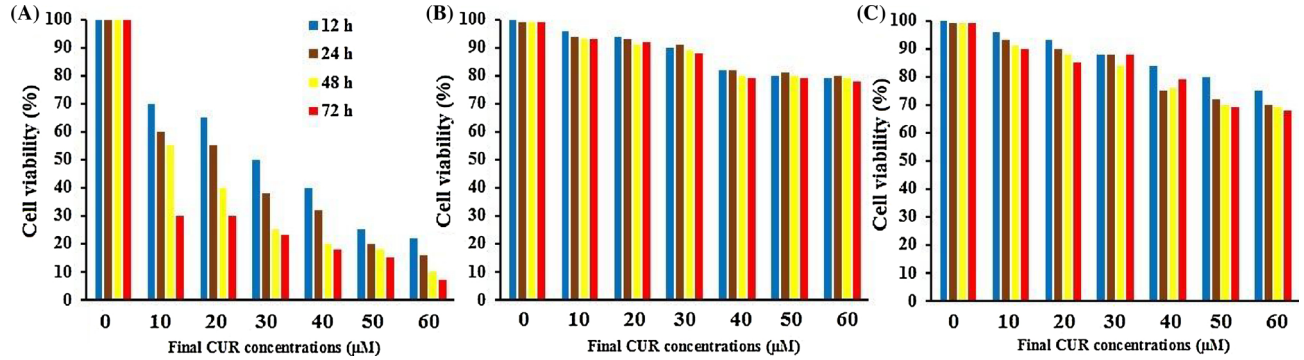

Fig. 8. The cytotoxicity effects of CUR@[As-PEGylated MSN@GO] nanohybrid on MCF-7 as cancerous cells (A) and MCF10A as normal cell (B) and the cytotoxicity effects of free CUR on MCF-7 cells.

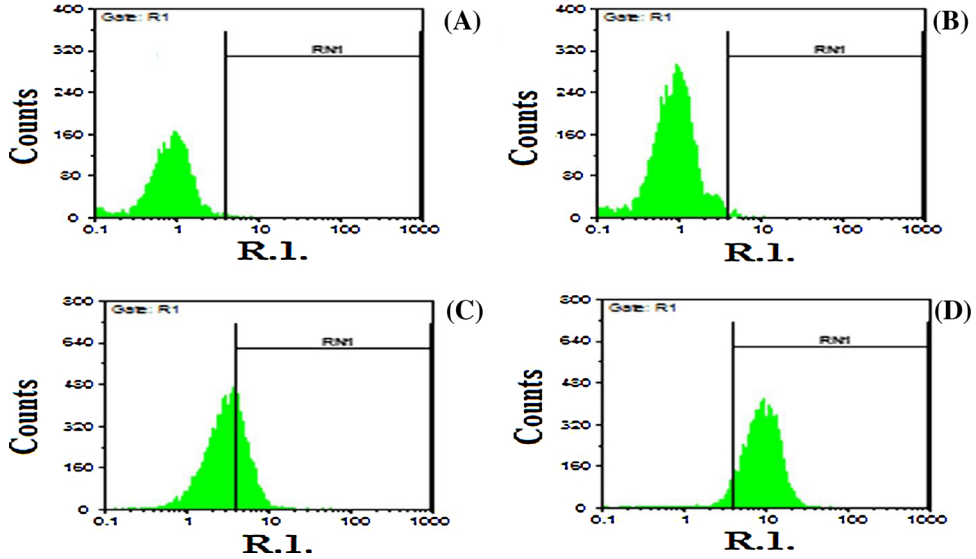

Fig. 9. Cellular uptake of a) autofluoresence of MCF-7 cells; b) curcumin drug; C) MCF-7 cells incubated with CUR; D) MCF-7 cells incubated with CUR@[As-PEGylated MSN@GO] nanohybrid, by flow cytometry.

condition). The CUR release efficiencies uniformly increased and reached to about 56% and 90% after 100 h under normal and acidic conditions, respectively. These results demonstrated that the releasing profile of CUR under acidic condition is much higher than normal pH and therefore CUR@[As-PEGylated MSN@GO] nanohybrid will be more efficient in cancerous cell environments.

3.4. Cell viability

Fig. 8 presents the cytotoxicity effects of CUR@[As-PEGylated MSN@GO] nanohybrid on MCF-7 (a) and MCF10A (b). *In vitro* investigation of the toxicity of CUR@[As-PEGylated MSN@GO] nanohybrid in these experiments were performed using MTT assay. The IC50 value of CUR@[As-PEGylated MSN@GO] nanohybrid for MCF-7 cell lines within 12, 24, and 48 h were 30, 21.5 and 15 μM, respectively. This value is also reduced to 14 μM after 72 h. In contrast, the same concentrations of CUR@[As-PEGylated MSN@GO] nanohybrid did not affect the proliferation of MCF10A cells. This observation can obviously verify the safety and biocompatibility of CUR@[As-PEGylated MSN@GO] nanohybrid.

3.5. Cellular uptake of NPs

Fig. 9 presents the uptake quantitative analysis of nanohybrid by flow cytometry. In this figure, the histograms of cellular fluorescence MCF-7 cells (a), CUR (b), MCF-7 cells incubated with CUR (c), and MCF-7 cells incubated with CUR@[As-PEGylated MSN@GO] nanohybrid (d) are displayed. According to Fig. 9a and b, the cells without CUR and nanoparticles (as a negative control), reveal only auto-fluorescence. However, a strong CUR fluorescence was revealed when MCF-7 cells were incubated with CUR (Fig. 9c), and MCF-7 cells were incubated with CUR loaded CUR@[As-PEGylated MSN@GO] nanohybrid (Fig. 9d). A higher uptake of CUR loaded nanohybrid in the breast cancer cells can be considered as an appropriate evidence for an improved therapeutic index.

4. Conclusions

Herein, a PEGylated functionalized mesoporous silica nanoparticles-graphene oxide hybrid has been fabricated by anchoring aspartic acid and PEG functional moieties onto the surface of MSN@GO scaffold as a biocompatible, and water-dispersed nanomaterial. Then, it has been evaluated as an effective and pH-controlled nano-carrier for improving the delivery of CUR to cancerous cell lines. Indeed, the structure of As-PEGylated MSN@GO nano-carrier was fully characterized and confirmed by a variety of techniques. Then, CUR was loaded on the surface of modified MSN@GO nanohybrid. MTT assay and flow cytometry techniques were applied to assay the efficiency and cellular uptake of CUR@[As-PEGylated MSN@GO] nanohybrid as an anticancer. Our data suggest that CUR@[As-PEGylated MSN@GO] nanohybrid has more cytotoxic effect on MCF-7 as the cancerous model cell *versus* pure CUR. Consequently, the loading of CUR onto As-PEGylated MSN@GO

nanohybrid is a considerable modification to overcome the short half-life and instability of CUR under normal conditions in order to raise the CUR capabilities to be utilized in the cancer therapy.

Conflict of interests

The authors declare no conflict of interests.

Financial disclosure

The authors have no funding to disclose.

References

[1] Liechty WB, Kryscio DR, Slaughter BV, Peppas NA. Polymers for drug delivery systems. Annu Rev Chem Biomol Eng 2010;1:149–73.
[2] Maheshwari RK, Singh AK, Gaddipati J, Srimal RC. Multiple biological activities of curcumin: a short review. Life Sci 2006;78:2081–7.
[3] Gupta SC, Patchva S, Koh W, Aggarwal BB. Discovery of curcumin, a component of golden spice, and its miraculous biological activities. Clin Exp Pharmacol Physiol 2012;39:283–99.
[4] Verderio P, Bonetti P, Colombo M, Pandolfi L, Prosperi D. Intracellular drug release from curcumin-loaded PLGA nanoparticles induces G2/M block in breast cancer cells. Biomacromolecules 2013;14:672–82.
[5] Ma'mani L, Nikzad S, Kheiri-manjili H, al-Musawi S, Saeedi M, Askarlou S, et al. Curcumin-loaded guanidine functionalized PEGylated I3ad mesoporous silica nanoparticles KIT-6: practical strategy for the breast cancer therapy. Eur J Med Chem 2014;83:646–54.
[6] Kheiri Manjili H, Ma'mani L, Tavaddod S, Mashhadikhan M, Shafiee A, Naderi-Manesh HD. L-sulforaphane loaded Fe3O4@ gold core shell nanoparticles: a potential sulforaphane delivery system. PLoS One 2016;11:e0151344.
[7] Mun S-H, Joung D-K, Kim Y-S, Kang O-H, Kim S-B, Seo Y-S, et al. Synergistic antibacterial effect of curcumin against methicillin-resistant Staphylococcus aureus. Phytomedicine 2013;20:714–8.
[8] Altaf SD, Bharat BA, Anupam B. Curcumin and liver cancer: a review. Curr Pharm Biotechnol 2012;13:218–28.
[9] Wuthi-udomlert M, Grisanapan W, Luanratana O, Caichompoo W. Antifungal activity of Curcuma longa grown in Thailand. Southeast Asian J Trop Med Public Health 2000;31(Suppl. 1):178–82.
[10] Ravindranath V, Chandrasekhara N. Metabolism of curcumn-studies with [3H] curcumin. Toxicology 1981;22:337–44.
[11] Aggarwal BB, Kumar A, Bharti AC. Anticancer potential of curcumin: preclinical and clinical studies. Anticancer Res 2003;36:3–98.
[12] Stankovich S, Dikin DA, Dommett GHB, Kohlhaas KM, Zimney EJ, Stach EA, et al. Graphene-based composite materials. Nature 2006;442:282–6.
[13] Schedin F, Geim AK, Morozov SV, Hill EW, Blake P, Katsnelson MI, et al. Detection of individual gas molecules adsorbed on graphene. Nat Mater 2007;6:652–5.
[14] Liu Q, Shi J, Sun J, Wang T, Zeng L, Jiang G. Graphene and graphene oxide sheets supported on silica as versatile and high-performance adsorbents for solid-phase extraction. Angew Chem 2011;123:6035–9.
[15] Xu G, Chen X, Hu J, Yang P, Yang D, Wei L. Immobilization of trypsin on graphene oxide for microwave-assisted on-plate proteolysis combined with MALDI-MS analysis. Analyst 2012;137:2757–61.
[16] Shan C, Yang H, Han D, Zhang Q, Ivaska A, Niu L. Water-soluble graphene covalently functionalized by biocompatible poly-l-lysine. Langmuir 2009;25:12030–3.
[17] Dong H, Zhu Z, Ju H, Yan F. Triplex signal amplification for electrochemical DNA biosensing by coupling probe-gold nanoparticles–graphene modified electrode with enzyme functionalized carbon sphere as tracer. Biosens Bioelectron 2012;33:228–32.
[18] Aliabadi M, Shagholani H, Yunessnia lehi A. Synthesis of a novel biocompatible nanocomposite of graphene oxide and magnetic nanoparticles for drug delivery. Int J Biol Macromol 2017;98:287–91.
[19] Subramanian AP, Jaganathan SK, Supriyanto E. Overview on in vitro and in vivo investigations of nanocomposite based cancer diagnosis and therapeutics. RSC Adv 2015;5:72638–52.
[20] Tang Y, Hu H, Zhang MG, Song J, Nie L, Wang S, et al. An aptamer-targeting photoresponsive drug delivery system using off-on graphene oxide wrapped mesoporous silica nanoparticles. Nanoscale 2015;7:6304–10.
[21] Slowing II, Trewyn BG, Giri S, Lin VSY. Mesoporous silica nanoparticles for drug delivery and biosensing applications. Adv Funct Mater 2007;17:1225–36.
[22] Guardia L, Suárez-García F, Paredes JI, Solís-Fernández P, Rozada R, Fernández-Merino MJ, et al. Synthesis and characterization of graphene–mesoporous silica nanoparticle hybrids. Microporous Mesoporous Mater 2012;160:18–24.
[23] Yang S, Feng X, Wang L, Tang K, Maier J, Müllen K. Graphene-based nanosheets with a sandwich structure. Angew Chem Int Ed 2010;49:4795–9.
[24] Wang Z-M, Wang W, Coombs N, Soheilnia N, Ozin GA. Graphene oxide-periodic mesoporous silica sandwich nanocomposites with vertically oriented channels. ACS Nano 2010;4:7437–50.
[25] Wang X, Pei Y, Lu M, Lu X, Du X. Highly efficient adsorption of heavy metals from wastewaters by graphene oxide-ordered mesoporous silica materials. J Mater Sci 2015;50:2113–21.
[26] Wang X, Liu J, Liu A, Liu Q, Du X, Jiang G. Preparation and evaluation of mesoporous cellular foams coating of solid-phase microextraction fibers by determination of tetrabromobisphenol A, tetrabromobisphenol S and related compounds. Anal Chim Acta 2012;753:1–7.
[27] Coasne B, Galarneau A, Pellenq RJM, Di Renzo F. Adsorption, intrusion and freezing in porous silica: the view from the nanoscale. Chem Soc Rev 2013;42:4141–71.
[28] El-Safty SA. Organic–inorganic hybrid mesoporous monoliths for selective discrimination and sensitive removal of toxic mercury ions. J Mater Sci 2009;44:6764.
[29] Asefa T, Tao Z. Biocompatibility of mesoporous silica nanoparticles. Chem Res Toxicol 2012;25:2265–84.
[30] Hudson SP, Padera RF, Langer R, Kohane DS. The biocompatibility of mesoporous silicates. Biomaterials 2008;29:4045–55.
[31] Lu J, Liong M, Li Z, Zink JI, Tamanoi F. Biocompatibility, biodistribution, and drug-delivery efficiency of mesoporous silica nanoparticles for cancer therapy in animals. Small 2010;6:1794–805.
[32] Yoo E, Okata T, Akita T, Kohyama M, Nakamura J, Honma I. Enhanced electrocatalytic activity of Pt subnanoclusters on graphene nanosheet surface. Nano Lett 2009;9:2255–9.
[33] Du Y, Guo S, Dong S, Wang E. An integrated sensing system for detection of DNA using new parallel-motif DNA triplex system and graphene–mesoporous silica–gold nanoparticle hybrids. Biomaterials 2011;32:8584–92.